A review on Light Extinction Spectrometry as a diagnostic for dust particle characterization in dusty plasmas

Séverine Barbosa, Fabrice R. A. Onofri, Lénaïc Couëdel, Mariusz Wozniak, Cédric Montet, Chantal Pelcé, Cécile Arnas, Laïfa Boufendi, Eva Kovacevic, Johannes Berndt, et al.

A review on Light Extinction Spectrometry as a diagnostic for dust particle characterization in dusty plasmas

S. BARBOSA[1], F. R. A. ONOFRI[1] †, L. COUEDEL[2], M. WOZNIAK[1*], C. MONTET[1], C. PELCE[1], C. ARNAS[2], L. BOUFENDI[3], E. KOVACEVIC[3], J. BERNDT[3], AND C. GRISOL I A[4]

[1] Université Aix-Marseille, CNRS, UMR 7343, IUSTI, 13458 Marseille Cédex 13, FRANCE
[2] Université Aix-Marseille, CNRS, UMR 7345, PIIM, 13397 Marseille Cédex 20, FRANCE
[3] Université d'Orléans, CNRS, UMR 6606, GREMI, 45000 Orléans, FRANCE
[4] CEA, IRFM, F-1308 Saint-Paul-lez-Durance, France
[*]Present affiliation: Institute of Physics, Polish Academy of Sciences, 02-668, Warsaw, Poland

(Received ?; revised ?; accepted ?. - To be entered by editorial office)

In this article, a detailed description of the light extinction spectrometry diagnostics is given. It allows the direct in-situ measurement of the particle size distribution and absolute concentration of a dust cloud levitating in plasmas. Using a relatively simple and compact experimental set-up, the dust cloud parameters can be recovered with a good accuracy making minimum assumptions on their physical properties. Special emphasises are given to the inversion of light extinction spectra and all the required particle shape, refractive index and the light extinction models. The parameter range and the limitations of the diagnostic are discussed. In addition, two examples of measurements in low-pressure gas discharges are presented: in a DC glow discharge in which nanoparticles are growing from the sputtering of a tungsten cathode, and in an Argon-Silane radio-frequency discharge.

1. Introduction

The knowledge of nano-(micro-) particle (commonly referred as "dust particles") parameters in a dusty plasma is essential for a genuine comprehension of the system. Indeed, as the dust particles acquire a net electric charge (usually negative) due to their interactions with the surrounding plasma electrons and ions, the discharge and plasma parameters can be strongly modified. Moreover the forces acting on the dust particles at the origin of their transport are highly dependent on the local plasma properties and thus retroactively depend on the dust size distribution and number density. In low-pressure gas discharges in which nanoparticles are growing (e.g. (Boufendi & Bouchoule 1994; Samsonov & Goree 1999*a*,*b*; Berndt *et al.* 2009; Dominique & Arnas 2007; Kishor *et al.* 2013; Hong *et al.* 2003)), the characterisation of the dust particle cloud is always one of the major issues. In many experiments, the measurements of the particle size distribution (PSD) and number density rely on ex-situ measurements using electron microscopes. For instance, Figure 1 shows electron microscopy images of particles with a wide variety of morphologies: porous and cauliflower-shape particles (Figure 1(a-b)), compact aggregates (Figure 1(c-e)) or even low fractal dimension aggregates (Figure 1(f)).

The evolution of the PSD is recovered by collecting particles for different discharge

† Email address for correspondence: fabrice.onofri@univ-amu.fr

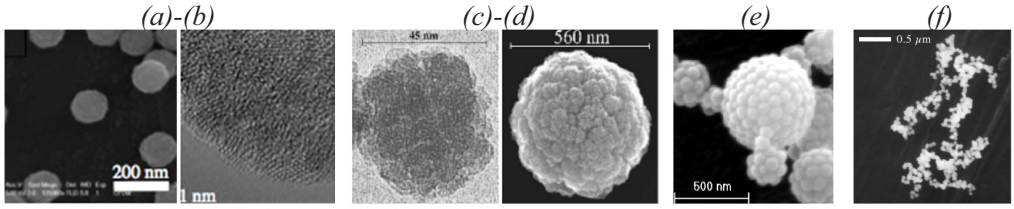

FIGURE 1. Electron microscopy images of particle aggregates formed in a DC Argon glow discharge: (a) SEM, (b) HR-TEM (Tungsten (Kishor *et al.* 2013)); an Argon-Silane low pressure radio-frequency plasma: (c) TEM, (d) SEM (silicon (Boufendi & Bouchoule 1994)); (e) an aerosol drier (SEM, silicon dioxide (Onofri *et al.* 2013)) and (f) sputtering discharge (SEM, aluminium (Samsonov & Goree 1999*b*)).

durations. Then, correlations are made with the evolution of the discharge parameters (Wattieaux *et al.* 2011), such as the self-bias voltage and current harmonics in radio-frequency (RF) discharges, the evolution of the cathode bias in direct-current argon glow discharge and, in many experiments, the plasma light emission. However, techniques relying on ex-situ measurements are very time consuming and not adapted when real-time in-situ knowledge of the PSD and number concentration are required. Recently, real-time evolution of the dust particle size and number concentration was obtained in capacitively-coupled RF discharges by following the electric parameters (RF current and voltage, self-bias) and deducing the modification of the plasma impedance. However, the recovery of the dust particle size and number concentration rely on modelling and a careful calibration of the considered set-up. Moreover, it is restricted to monodisperse spherical particles and cannot properly handle dust particles with complex shapes and polydisperse PSD. Laser light scattering on the dust particles is often used to observe in-situ and in real time the nanoparticle cloud. It is however very difficult to extract the evolutions of the PSD and number concentration from the scattering signals as they depend on too many parameters (particle size and shape, number concentration, refractive index) and require observations from many angles. Mie-scattering ellipsometry (Gebauer & Winter 2003; Hong & Winter 2006; Sebastian *et al.* 2015) seems to be more accurate diagnostic. It consists in measuring the change of polarisation of a polarised laser-light beam scattered by a cloud of nanoparticles. Coupled with extinction, it allows recovering the PSD and the number concentration. It is however experimentally challenging, as it requires accurate measurements of the ellipsometric angles. The iterative data procedure used to find the particle parameters (PSD, local density, and refractive index) is also not trivial and generally requires strong assumptions making systems with complex shaped particle and polydisperse PSD complicated to handle. Otherwise, a reduction of the number of parameters can be considered. For example, the choice of a model providing the time evolution of the particle radius can help in this way. Dust particle size evolution can also be followed, for instance, by measuring white light scattering at different angles (Mitic *et al.* 2011). By looking at the ratio of the scattered light at different angles for given wavelengths, it is possible to recover the particle size and the refractive index. This technique however assumes that the particles are spherical and monodisperse.

In this article, we will focus and review on the basic principle, recent achievements and applications of a diagnostic: the Light Extinction Spectrometry (LES), for the in-situ measurement of the PSD and concentration of dust cloud levitating in plasmas. LES uses the extinction of a collimated broadband light beam to recover the PSD and the absolute concentrations in number and in volume of dust levitating in plasmas. Under appropriate conditions, it has the capability to detect nanoparticles as small as 20 nm,

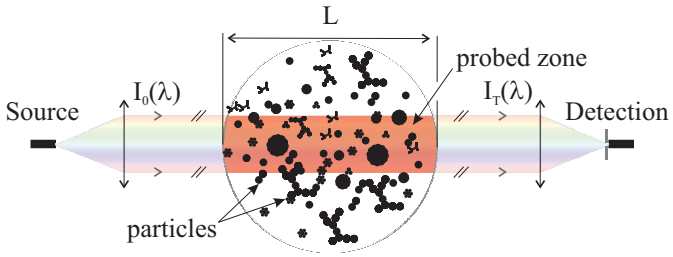

FIGURE 2. Schematic of the principle of light extinction spectroscopy.

to handle rather complex shaped particles as well as multimodal size distributions. LES is effectively used to measure PSDs and particle concentrations in plasmas, aerosols and colloidal suspensions (Crawley *et al.* 1997; Tamanai *et al.* 2006; Rosanvallon *et al.* 2008, 2009; Onofri *et al.* 2009, 2011, 2013; Barbosa *et al.* 2016). The remainder of this paper is organized as follows. In section 2, the bases of the LES are introduced. Special emphasises are given to the inversion of light extinction signals and all the necessary particle shape, refractive index and light extinction models. Section 3 discusses the parameter range and the limitations of LES. Finally, section 4 gives two examples of measurements in low-pressure gas discharges: a DC glow discharge in which particles are growing from the sputtered from a tungsten cathode, and a CC-RF discharge using a mixture of argon and silane to grow silicon particles.

2. Summary of Light Extinction Spectroscopy (LES) method

2.1. *Physical basis and basic equations*

LES consists in analyzing the variations of the spectral transmittance of a broadband and collimated light beam passing through the particle cloud to be characterized (e.g. (Bohren & Huffman 1998; Xu 2001; Onofri & Barbosa 2012*b*)), see Figure 2.

Considering I_0 and I_T, the spectral intensities of the illuminating and transmitted beams respectively, the light beam spectral transmittance $T(\lambda)$, also called transmission, is defined as follows:

$$T(\lambda) = \frac{I_T(\lambda) - I_b(\lambda)}{I_0(\lambda) - I_b(\lambda)} \tag{2.1}$$

where λ is the considered light wavelength and I_b accounts for the noise of the detection system (e.g. electronic dark noise of the spectrometer, residual background optical noise of the laboratory and plasma light emission). If the contribution of the light scattered in the forward direction by the dust cloud can be neglected, the measured transmission is simply an exponentially decreasing function $T(\lambda) = \exp(-\tau)$ of the optical thickness $\tau = C_n\overline{C_{ext}}L$ of the particle cloud. In the latter relation, C_n stands for the particle concentration in number, L is the length of the probed zone and $\overline{C_{ext}}$ is an integral quantity representing the particle size and spatially averaged extinction of the particle in the probed zone:

$$\overline{C_{ext}} = \int_{D_{min}}^{D_{max}} C_{ext}(D, \tilde{m})\, n(D) dD \tag{2.2}$$

where C_{ext} is the extinction cross-section of a single particle with diameter D and complex refractive index $\tilde{m}(\lambda)$; D_{min} and D_{max} are the diameter of the smallest and the largest particles respectively, and n the normalized particle size distribution (PSD) in number.

C_{ext} is the sum of two distinct contributions: $C_{ext} = C_{abs} + C_{sca}$, with C_{abs} and S_{sca} the particle absorption and scattering cross-sections, respectively.
For spherical particles, C_{ext} can be expressed as :

$$\overline{C_{ext}} = \int_{D_{min}}^{D_{max}} Q_{ext}\left(D, \lambda, \tilde{m}\right) \frac{\pi D^2}{4} n(D) dD \tag{2.3}$$

where $Q_{ext} = 4C_{ext}/\pi D^2$ is the extinction coefficient of a single particle. The concentration in volume C_v and the normalized PSD in volume v can be derived straightfowardly from the corresponding quantities in number:

$$V(D) = C_v v(D) = \frac{\pi C_n}{6} \int_{D_{min}}^{D_{max}} D^3 n(D) dD \tag{2.4}$$

with :

$$\int_{D_{min}}^{D_{max}} n(D) dD = \int_{D_{min}}^{D_{max}} v(D) dD = 1 \tag{2.5}$$

where V is the PSD in volume from which the PSD in mass can be deduced if the particle density is known. By replacing number quantities by volume ones and by introducing the constant $\Lambda = -3L/2$, LES transmission equation can be linearized as follows (Onofri *et al.* 2011):

$$ln\left[T\left(\lambda_i\right)\right] = \Lambda \int_{D_{min}}^{D_{max}} Q_{ext}\left(\lambda, D, \tilde{m}\right) \frac{V(D)}{D} dD \tag{2.6}$$

The equation 2.6 is an inhomogeneous Fredholm equation of the first kind (e.g. (Aster *et al.* 2012; Hansen *et al.* 2012)), which can be discretized to obtain an algebraic relation of the form $\widehat{\mathbf{T}} = \mathbf{SV}$, with:

$$\widehat{T}\left(\lambda_i\right) = ln\left[T\left(\lambda_i\right)\right] = \sum_{j=1}^{N} S_{i,j} V_j \tag{2.7}$$

where the quantity to be determined is a vector $\mathbf{V}$ with elements V_j and $j = 1, 2, ..., N$. N is the number of size classes (i.e. bins) used to discretize the PSD. $\mathbf{S}$ is a $M \times N$ matrix called (abusively) the extinction matrix. It is a discrete form of the kernel of the integral equation 2.6. Each of its elements $S_{i,j}$ represents the extinction coefficient divided by the particle diameter of the particle size class j for the wavelength λ_i, with $i = 1, 2, ...M$. M is the number of wavelengths (or spectral bands) used to discretize the logarithm of the transmittance spectrum (which vector form is noted herein $\widehat{\mathbf{T}}$, with elements $\widehat{T}_i$, to simplify the notations). The $M \times N$ elements of $\mathbf{S}$ are averaged over the width δ_D of the size classes and the width δ_λ of the spectral bands. If δ_D and δ_λ are constant, a simple midpoint rule can be used for the numerical quadrature (Hansen *et al.* 2012):

$$S_{i,j} = \frac{\Lambda}{\delta_D \delta_\lambda} \int_{D_j - \delta_D/2}^{D_j + \delta_D/2} \int_{\lambda_i - \delta_\lambda/2}^{\lambda_i + \delta_\lambda/2} Q_{ext}\left(\lambda_i, D_j, \tilde{m}\right) \frac{V(D)}{D} d\lambda dD \tag{2.8}$$

This quadrature method works fine until δ_λ and δ_D are small (i.e. the variations of $Q_{ext}(\lambda, D, \tilde{m})V(D)/D$ are negligible over the corresponding ranges). This implies that the dimensions and the condition number of the matrix $\mathbf{S}$ remain relatively large, which is not suitable for the inversion step (see §2.2). Depending of the application, it can be necessary to employ quadrature rules using more complex interpolating functions than a mean value (equation 2.8), like the trapezoidal rule (linear fit) or rules based on spline functions (Hansen *et al.* 2012), etc.

Equations 2.1, 2.2 are valid for any particle shape, while equation 2.3 is only valid for spherical particles. As a matter of fact, a parameter like the diameter is not necessarily sufficient, or the unique way, to classify non-spherical particles. It is agreed that the diameter of roughly spherical particles refers to the diameter of spherical particles having the same projected cross section, surface, volume or ratio of volume and surface (Mishchenko *et al.* 2000). In that case, the PSD retrieved from LES measurements is well defined and directly comparable with other results (TEM analyses for instance). However, these results may be not appropriate to estimate other properties of the particles (e.g. internal porosity and specific surface). In the case of dense aggregates for instance, it can be more appropriate to classify them in terms of number of monomers or radiuses of gyration (e.g. see §2.3 and Figure 4).

2.2. *Regularization and inversion procedure*

To retrieve the PSD and particle concentration from LES measurements, it is necessary to solve the algebraic equation $\widehat{\mathbf{T}} = \mathbf{SV}$. Unfortunately, the direct solution $\mathbf{V} = \left(\mathbf{S^t S}\right)^{-1} \mathbf{S^t} \widehat{\mathbf{T}}$ (where the superscripts t and -1 denote the matrix transpose and inverse operations respectively) is not of practical use since we are facing an ill conditioned problem (Hansen 1998; Tikhonov *et al.* 1995). The condition number of $\mathbf{S}$ is always so large that even numerical computation round-off errors are enough to strongly disturb the solution. Experimental LES spectra being inevitably contaminated by various noise sources (electronic, residual plasma emission, ect), obtaining a direct solution is unthinkable. Writing equation 2.6 in term of volume quantities rather than number ones helps in minimizing the condition number of $\mathbf{S}$. However this is still not sufficient to get a stable and reliable solution. The problem must be regularized. In other words, more physical inputs (i.e. *a priori*) and mathematical constraints must be injected into the problem. The literature on regularization methods is extremely dense and various solutions have been proposed (Tikhonov *et al.* 1995; Hansen 1994). In the following, we summarized the principle of two methods that were used to investigate particle growth in different low-pressure gas discharges (see §4 for applications) (Onofri *et al.* 2011; Barbosa *et al.* 2016).

A regularization method based on a dependant model assumes the shape of the PSD to be determined. This is clearly a strong assumption, which can lead to serious errors if the *a priori* is too far from the real solution. Conversely, since this method imposes a strong constraint on the solution that is sought, it is rather robust regarding the experimental noise and can be used to directly determine the PSD in number for instance. Such a method can be implemented with a non-negativity-constrained least squares algorithm (since all elements of a PSD are positives, $V > 0$) and a parametric estimator (also called a performance function) quantifying the quality of the reconstruction (Barbosa *et al.* 2016; Onofri *et al.* 2013). For a two-parameter distribution for instance, the mean diameter $\overline{D}$ and the corresponding standard deviation σ_D are the two unknowns of the problem. The latter can be determined iteratively using a χ^2-test for the parametric estimation. In that case, the quantity to minimize may be expressed as:

$$\chi^2\left(\overline{D}, \sigma_D\right) = \sum_{i=1}^{N} \left(\frac{\widehat{T}_i - S_{i,j} V_j(D_j; \overline{D}, \sigma_D)}{\sigma_\omega(\widehat{T}_i)} \right) \tag{2.9}$$

where $\widehat{T}_i$ represents an element of the experimental spectrum and the product $S_{i,j}V_j$ the corresponding modeled quantity obtained for the iteration parameters $\overline{D}$ and σ_D. The statistical weighting coefficients $\sigma_\omega(\widehat{T}_i)$ allow to give a higher weight to the spectral bands in which we are more confident. They can be estimated from the analysis of the signal-to-noise ratio (SNR) or, more simply, from the standard deviation of a

set of LES spectra. If not possible, they are set to be equal to unity. Many fittings models can be used *a priori*, like the Normal, the Log-normal, the Gamma distribution, etc. (Xu 2001; Mishchenko *et al.* 2000). The Normal distribution is mostly used for quasi-monodisperse particulate medium, while the Log-normal is preferably used for polydisperse systems. As a rule, it is also required to iterate on the limits D_{min} and D_{max}. This is time consuming and hazardous when there is little knowledge about the particle cloud properties. To overcome this difficulty, D_{min} and D_{max} are often imposed via the definition of a cut-off, or an integral convergence criteria, on the PSD (Onofri *et al.* 2013; Mishchenko *et al.* 2000). In the case of the Log-normal distribution, these two parameters can be defined as particle sizes for which the PSD equals 0.1%, i.e. $\{D_{min}; D_{max} | n_{lnN}(D_S; \mu, \sigma)/exp(\mu - \sigma^2) = 0.001\}$ (Onofri *et al.* 2013). When a bimodal distribution is expected for instance, the iteration is performed on the parameters of the two individual distributions, $\overline{D}_1$, $\sigma_{D,1}$ and $\overline{D}_2$, $\sigma_{D,2}$, plus on the relative weight α of the two modes: $n\left(D; \overline{D}_1, \sigma_{D,1}, \overline{D}_2, \sigma_{D,2}, \alpha\right) = \alpha n\left(D; \overline{D}_1, \sigma_{D,1}\right) + (1-\alpha) n\left(D; \overline{D}_2, \sigma_{D,2}\right)$ with $0 < \alpha < 1$ (Barbosa *et al.* 2016). Note that the two distributions are not necessarily of the same type and they can overlap (see 4.1).

The constrained linear inversion method exists in various forms: Tikhonov regularization (Tikhonov *et al.* 1995), truncated singular value decomposition (Hansen *et al.* 2012), Phillips-Twomey (Phillips 1962; Twomey 1963, 1979) methods,... which are all equivalent (Hansen 1998). For historical reasons, the PhillipsTwomey method is the most widely used in the field of optical particle characterization (e.g. (Xu 2001; Sentis 2014; Glasse *et al.* 2015; Wyatt *et al.* 1988)). This method allows for more measurements than unknowns (i.e. $N < M$), but the opposite is also possible (i.e. $N > M$). With the original Phillips-Twomey , the solution can be directly obtained from a single matrix inversion:

$$\mathbf{V} = \left(\mathbf{S^t S} + \gamma \mathbf{H}\right)^{-1} \mathbf{S^t} \widehat{\mathbf{T}} \tag{2.10}$$

where $\mathbf{H}$ is a $M \times M$ smoothing matrix and γ a smoothing parameter (also called Lagrange multiplier). The uncertainties of non-correlated measurements can be taken into account via a diagonal matrix $\mathbf{S_w}$ whose elements are, for instance, the quantities $1/\sigma_\omega(\widehat{T}_i)$. In the latter case, the solution is obtained from:

$$\mathbf{V} = \left(\mathbf{S^t S_\omega^{-1} S} + \gamma \mathbf{H}\right)^{-1} \mathbf{S^t S_\omega^{-1}} \widehat{\mathbf{T}} \tag{2.11}$$

The vector $(\mathbf{S^t S_\omega^{-1} S} + \gamma \mathbf{H})^{-1}$ provides an estimation of the uncertainties into the solution (King *et al.* 1978). Although, equation 2.10 provides an explicit solution to the problem, it is preferable to minimize, in the least square sense, the difference between the measured and the modeled quantities:

$$\mathbf{V} = \left\{ \mathbf{V} | \underset{\mathbf{V>0}}{\mathrm{Min}} \left\{ \left| \left(\mathbf{S^t S} + \gamma \mathbf{H}\right) \mathbf{V} - \mathbf{S^t} \widehat{\mathbf{T}} \right|^{\mathbf{2}} \right\} \right\} \tag{2.12}$$

Depending on the problem and the *a priori* knowledge available on the expected PSD (e.g sharpness or smoothness) the identity matrix or an approximation to the first or second derivative operator can be chosen for $\mathbf{H}$ (Hansen 1994; Glasse *et al.* 2015). The analysis of numerically generated synthetic LES spectra (assuming $\mathbf{V}$, and calculating $\mathbf{SV}$) is used for this purpose. The selection of the smoothing parameter is more difficult. Excessive values of γ tend to over regularize the solution (which is then excessively low-pass filtered), while too small values of this parameters cannot stabilize the solution (which takes the form of a sum of Dirac-like distributions). Over the different methods available to estimate the optimal value of the regularization parameter (Aster *et al.* 2012; Hansen 1998), the L-Curve method (Hansen *et al.* 2012; Hansen 1994) is certainly the

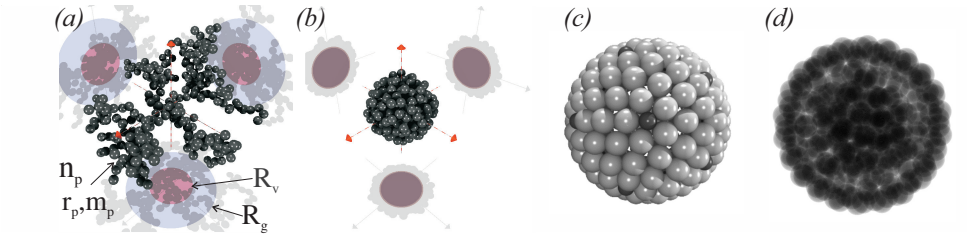

FIGURE 3. Numerically generated aggregates. Fractal aggregates composed of 300 monomers with (a) $D_f = 2.00$ and with (b) $D_f = 2.85$ (Onofri *et al.* 2011). Buckyball shaped aggregate of 162 monomers with a regular pentagonal-hexagonal surface lattice and a 3D hexagonal compact internal structure: (c) reflection and (d) transmission images (Onofri *et al.* 2013).

more comprehensive: the norm of the retrieved solution $|\mathbf{V}_\gamma|^\mathbf{2}$ is plotted versus the residual norm $\left|(\mathbf{S^t S} + \gamma\mathbf{H})\mathbf{V} - \mathbf{S^t}\widehat{\mathbf{T}}\right|^2$ for a large range of values for γ. The result is expected to take the form of a L-shaped curve. The optimal value of γ is the one minimizing at the same time the norm of the retrieved solution and the norm of the residual, i.e. the value associated to the corner of the L-curve obtained (Hansen 1994).

2.3. *Particle shape and refractive index models*

The particle morphology is a key factor for many obvious reasons, and this is particularly true for LES, since it is an input of the electromagnetic models used to calculate the extinction matrix. As pointed out in the introduction (§1), in reactive plasmas, dust particle clouds are often composed of monomers and their aggregates. To describe these particles, most studies used the spherical shape model. This choice can be justified when monomers are roughly spherical and their aggregates highly compact. It is however more doubtful to choose this particle shape model when nothing is known about the particle or when a more realistic model would involve too many unknowns.

A simple and relatively inexpensive approach to model aggregates of monomers is to use the so-called fractal-aggregate equation: $n_p = k_f\,(R_g/r_p)^{D_f}$ (Witten & Sander 1981; Sorensen 2001; Theiler 1990; Wozniak *et al.* 2012; Wozniak 2012). In the latter power-law equation, n_p and r_p stand for the number and radius of monomers within the aggregate respectively, while k_f, D_f and R_g are the aggregate prefactor, fractal dimension and radius of gyration (i.e. monomers mean square distance from the centre of mass of the whole aggregate) respectively. There exist several approaches to numerically generate fractal-like aggregates (Theiler 1990; Kaye 1994; Meakin 1983; Jullien & Botet 1987). A tunable Diffusion Limited Aggregation (DLA) (Witten & Sander 1981) model is probably the most efficient method to produce aggregates with well defined parameters. A code like DLA 1.13 (Wozniak *et al.* 2012; Wozniak 2012; Mroczka *et al.* 2012; Wozniak & Onofri 2012) allows, for instance, the simulation of fractal-aggregates composed of thousands of polydisperse, multi-material and overlapping (i.e. partially melt) monomers. This code can also provides reflection (e.g. SEM-like) or transmission (e.g. TEM-like) images of these aggregates (Wozniak *et al.* 2012). As an example, Figure 3(a-b) show for two synthetic aggregates composed of the same number of monomers: 3D rendering views (with POV-Ray (POV-Ray 2010)) and native 2D projections showing the radius of gyration and the radius in volume of the equivalent spheres. The monomers observed in plasma systems are obviously not always spherical and their aggregates not well described by the fractal equation. In that case, it is necessary to develop a dedicated particle shape model using the analysis of SEM/TEM images. It can be based on some dendrite growth

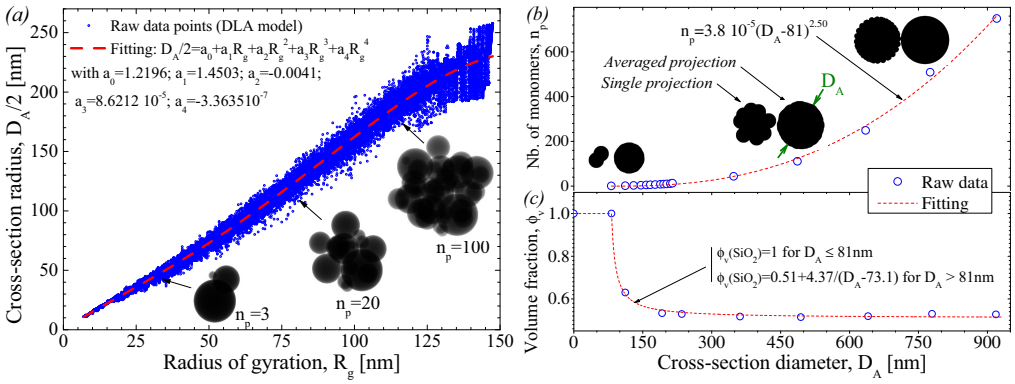

FIGURE 4. Numerically generated aggregates - polynomial regression models: (a) evolution of the cross-section radius of aggregates with the same fractal dimension ($D_f = 2.85$) versus their gyration radiuses OAPlum12; (b) evolution of the number of monomers and (c) the volume fraction of buckyball shaped aggregates versus their cross-section diameter (Onofri *et al.* 2013).

mechanisms (Aster *et al.* 2012), a Gaussian sphere model (Muinonen *et al.* 1996) or simple geometrical considerations (Onofri *et al.* 2013). Figure 3(c-d) show for instance the reflection and transmission images of a buckyball shaped aggregate exhibiting a regular pentagonal-hexagonal surface lattice (see also Figure 1(e)). The outputs of all particle shape models are also useful to link together the different parameters of the aggregates (as shown in Figure 4). The inset images in Figure 4(a) represent 2D projections of three particular fractal aggregates over the 25000 generated to obtain a polynomial regression model relating the aggregate cross-section diameter $D_A = 2\sqrt{A/\pi}$ to their radius of gyration (Onofri *et al.* 2012). In the latter relation, A stands for the statistically averaged 2D projected area of aggregates having the same morphological parameters. Figure 4(b-c) show similar results for buckyball shaped aggregates with, in addition, the evolution of their volume fraction ϕ_V in monomers ($1-\phi_V$ represents the aggregate porosity) (Onofri *et al.* 2013).

The particle complex refractive index $\tilde{m}$ is also a key input of electromagnetic models. It is a crucial parameter for all light diagnostics, but this is particularly true for LES. In fact, in contrast to multi-angle or ellipsometry techniques (e.g. (Hong & Winter 2006; Xu 2001; Sentis *et al.* 2014)), LES requires the knowledge of the particle material refractive index over a large spectral bandwidth and not only for a single (laser) wavelength. This is clearly one of the main drawbacks of this technique and especially when dealing with multi-component materials such as those produced in fusion plasma devices for instance (Onofri *et al.* 2009; Sharpe *et al.* 2002). Different strategies exist for solving this issue. Firstly, it is possible to collect in the literature and in on-line databases the refractive index spectra of various materials (i.e. Be, Si, SiC, W, WO_3,...) (Palik 1997; SOPRA 2008; Jäger *et al.* 2003). This procedure requires some *a priori* knowledge, or some prior analysis of the composition of particle samples. The particle refractive index is assumed to be identical to the one of the bulk material. Secondly, multi-components materials can be modeled using effective medium approximations like the Maxwell-Garnett or the Bruggeman relations (Bohren & Huffman 1998; Bohren 1986). These approximations provide effective electrical permittivities (an thus, the refractive indexes) for materials with embedded inclusions. The latter are expected to be small compared to the wavelength and with a moderate relative refractive index. These approximations, whose validity was

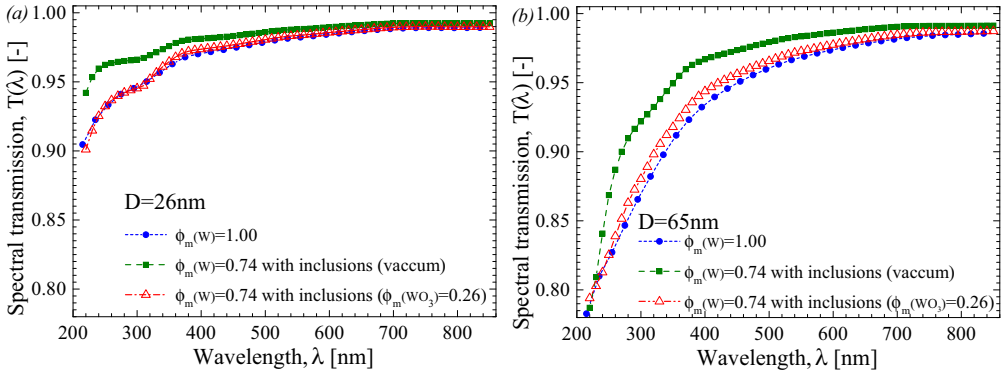

FIGURE 5. Numerical prediction with the Lorenz-Mie theory and Maxwell-Garnett effective medium approximation of the transmission of a cloud of monodisperse spherical particles with diameter (a) $D = 26$ nm , (b) $D = 65$ nm. Three particle compositions are considered: pure tungsten (mass fraction, $\phi_m(W) = 1$), porous tungsten (e.g. vacuum or gas inclusions, $\phi_m(W) = 0.74$), tungsten with tungsten oxide inclusions ($\phi_m(W) = 0.74$, $\phi_m(WO_3) = 0.26$). The particle concentration is fixed to $C_n = 10^{13}$ m^{-3} for a probing length of $L = 1$ m (Barbosa *et al.* 2016).

recently demonstrated (Mishchenko *et al.* 2014), were used, to evaluate changes in the scattering properties of carbonaceous particles contaminated by an increasing volume fraction of spherical inclusions of tungsten (Onofri *et al.* 2009), or the influence of the porosity or a partial oxidation of tungsten particles (Barbosa *et al.* 2016). Thirdly, this problem can also be partly handled by the scattering models themselves by deriving the effective refractive index of coated particles (Berndt *et al.* 2009), aggregates of spheres or electrical dipoles with different compositions (Onofri *et al.* 2009). Fourthly, the particle refractive index spectra can be determined experimentally by measuring the spectral hemispheric-reflectivity (ideally from deep UV to far infrared) of a particle sample. From these spectra the complex refractive index spectra can be reconstructed using KramersKronig integrals (Ku & Felske 1986). Finally, the PSD can be used as an input of the inversion method that is performed to retrieve the particle refractive index spectra.

2.4. *Calculation of the extinction matrix*

The calculation of the extinction of the so-called extinction matrix requires an accurate modeling of the particle absorption and scattering cross-sections. For this, as already mentioned, it is necessary to have appropriate particle shape and refractive index models, but also an accurate electromagnetic model. In what follows, a brief review is performed on the principal models relevant for LES (i.e. particle with size parameters in the range $x = \pi D/\lambda : 0.05 - 30$) (Bohren & Huffman 1998; Onofri & Barbosa 2012*a*; Wriedt 1998, 2010).

The Rayleigh-Debye-Gans approximation for fractal aggregates (RDG-FA) is a generalization of the well-known Rayleigh and Rayleigh-Debye-Gans approximations for optically soft scatterers ($x \equiv kR_g = 1$ and $|\tilde{m} - 1| = 1$, with $k = 2\pi/\lambda$). As an approximation, it gives simple analytic expressions for the cross-sections of fractal aggregates, with $C^a_{abs} = n_p C^p_{abs}$ for absorption and $C^a_{sca} = n_p^2 C^p_{sca} g(k, R_g, D_f)$ for scattering, (Guinier *et al.* 1995; Farias *et al.* 1996; Dobbins & Megaridis 1991). In the latter relations, the superscript a refers to the aggregate properties and the sub(super)script p refers to the properties of a single monomer, when $g(k, R_g, D_f)$ is a structure factor whose form de-

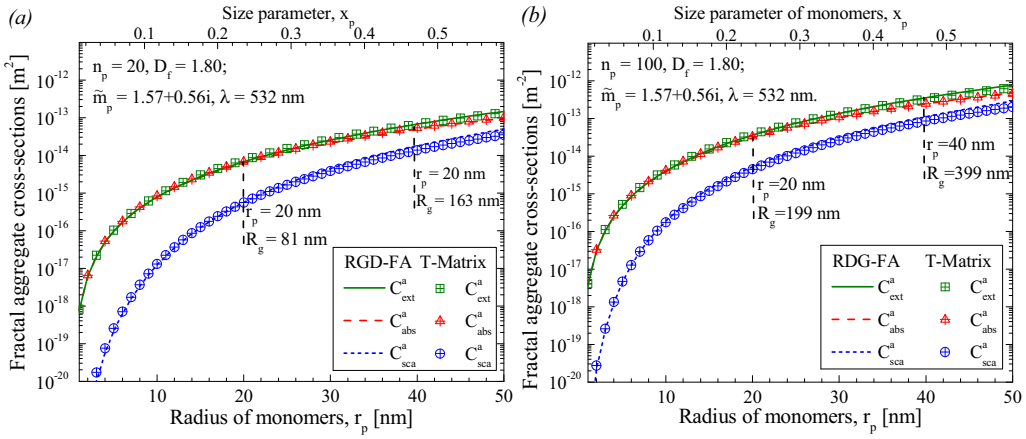

FIGURE 6. Comparison between RGD-FA and T-Matrix calculations (Wozniak 2012) for the cross-sections of carbonaceous aggregates of the same composition and morphology: $\tilde{m} = 1.56 + 0.57i$, $\lambda = 532$ nm, $D_f = 1.80$, for increasing radius of monomers with (a) $n_p = 20$ and (b) $n_p = 100$.

pends on whether the power-law regime is reached or not (i.e. the aggregate is sufficiently large with respect to the wavelength) (Mroczka *et al.* 2012). As RDG-FA neglects multiple scattering within the aggregates, its accuracy strongly decreases for high fractal dimension (e.g. compact aggregates like the ones shown in Figure 1(a-e)). Nonetheless, as shown in Figure 6, when compared to a rigorous electromagnetic model, RDG-FA provides reasonably accurate predictions for low fractal dimension aggregates (Wozniak *et al.* 2012; Chakrabarty 2009), e.g Figure 1(f). It is also computationally much more effective than rigorous electromagnetic models, e.g. it takes only few seconds with RDG-FA to get the results reported in Figure 6 when a tens hours are required with the T-Matrix (see below).

The Lorenz-Mie Theory (LMT, e.g. (Bohren & Huffman 1998)) solves the basic problem of the scattering of a plane electromagnetic waves by a non-magnetic, isotopic and homogeneous spherical particle (called a "Mie scatterer"). LMT has been extended during the last decades to account for arbitrary shaped beams as well as multilayered or chiral spheres (Onofri *et al.* 1995; Yan *et al.* 2012; Borghese *et al.* 1994), spheres with inclusions (Borghese *et al.* 1994), spheroids (Asano & Yamamoto 1975), etc. This theory uses a separation variable method to solve Maxwell's equations with the appropriate boundary conditions. Theoretically, it has no limitations in terms of particle size range and refractive index. Nonetheless, due to the difficulty in the calculation of complex functions with a large complex argument, the numerical difficulties appears for millimeter sized spherical and cylindrical particles, and a few tens of micrometers for other particle shapes. When coupled with effective medium theories, LMT can handle materials that are heterogeneous at the nanoscale, see Figure 7. In this example, the results obtained with the LMT and the Maxwell-Garnet approximation are in good agreement with rigorous electromagnetic calculations provided that the monomers (i.e. inclusions) remain much smaller than the illumination wavelength.

The T-Matrix method (T-Matrix)(Waterman 1965) is an integral method coming in two forms, the null field and extended boundary technique method e.g (Wriedt 2007; Mishchenko & Martin 2013). Its name refers to the calculation of a transformation matrix allowing to link, using boundary conditions on a circumscribing sphere, the internal field and scattered field that are expended in terms of spherical vector wave functions.

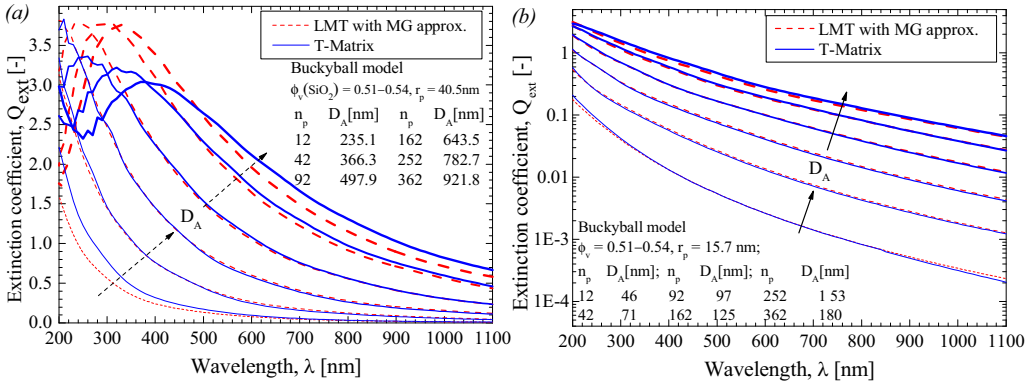

FIGURE 7. Comparison of the evolution of the extinction coefficient of dense buckyball shaped aggregates (of silica nanobeads): Lorenz-Mie theory with Maxwell-Garnett (MG) effective medium approximation versus T-Matrix calculations (Onofri *et al.* 2013).

Once this matrix is determined, all the particle extinction and scattering properties can be deduced. For numerical reasons, depending on the particle refractive index and shape (i.e. aspect ratio notably), this method is still limited to size parameters bellow $10 \sim 500$. Since it requires large computational resources, its results are mostly used in the form of look-up tables (i.e. **S** matrices for various particle shapes and compositions). As an illustration on T-Matrix capabilities (Mackowski & Mishchenko 1996; Mishchenko & Travis 2010), Figure 8 shows the spectral evolution of the normalized extinction coefficient Q^a_{ext}/Q^p_{ext} of clouds of amorphous silicon aggregates. In the limit of a low optical thickness of the particle cloud, the latter were simply simulated by averaging the extinction properties of 500 aggregates for each considered case (i.e., multiple scattering effects between different aggregates is neglected but not multiple scattering effects within the aggregates). In Figure 8(a) the fractal dimension increases from $D_f = 1.5$ (i.e. chain-like aggregates) to $D_f = 2.8$ (i.e. cauliflower-like aggregates) while the radius of gyration is kept constant $R_g = 35$ nm and the number of monomers increases from 51 to 1000. By contrast, in Figure 8(b) the fractal dimension is kept constant ($D_f = 2.85$) when the number of monomers increases from 11 to 1000 (i.e. R_g increases from 7 to 35 nm). As it can be seen, LES sensitivity to the particle morphology is quite low. This must be considered as positive when little is known on the particle cloud properties.

The Discrete Dipole Approximation (DDA) is a numerical method that solves the problem of the scattering and absorption by an array of polarizable point dipoles in interaction with a monochromatic plane wave (e.g. (Draine & Flatau 1994; Yurkin & Kahnert 2013)). The particle model, whose shape can be virtually arbitrary, is meshed with thousands or millions of dipoles. The counterpart of this flexibility is that this method requires larger computational facilities. It is also limited in terms of maximum particle size and refractive index (i.e. $|\tilde{m}|x < 0.5 \sim 1$ and $|\tilde{m} - 1| < 2$). The limit on the refractive index is the more problematic for LES. In fact, the complex refractive index of most material encountered in plasma devices is rather hig he UV range, precisely where the LES sensitivity to particle morphology is maxim

2.5. *Basic experimental set-up and software requirements*

A LES set-up comes in various forms (e.g. (Xu 2001; Onofri & Barbosa 2012*b*; Glasse *et al.* 2015; Deepak & Box 1978*a*; Crawley *et al.* 1997)). To give an illustration of a typical set-up, the authors present below their own diagnostic, see a schematic view on Figure 9.

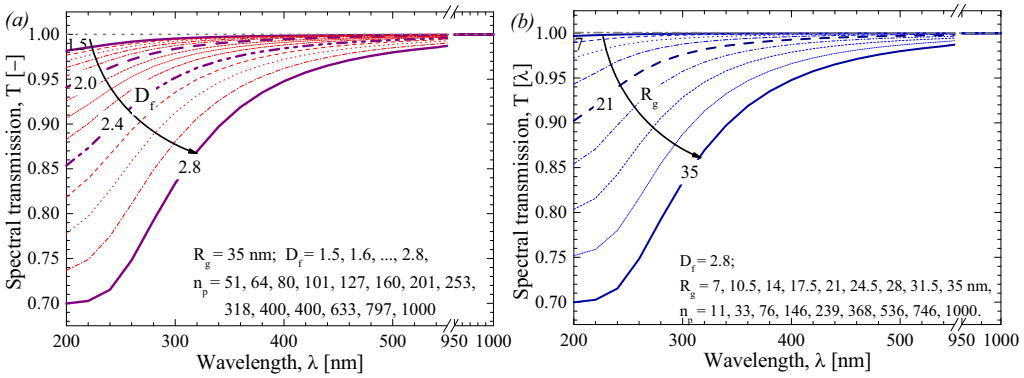

FIGURE 8. Numerical predictions with the T-Matrix method of the transmission of a cloud of fractal aggregates of amorphous silicon monomers with (a) the same radius of gyration but various fractal dimensions (and numbers of monomers) and (b) the same fractal dimension but various radiuses of gyration (and numbers of monomers). Other parameters are kept constant: $r_p = 3.5$ nm, $k_f = 1.593$, $C_n = 2.10^{13}$ m^{-3}, $L = 1$ m (Onofri *et al.* 2011; Wozniak 2012).

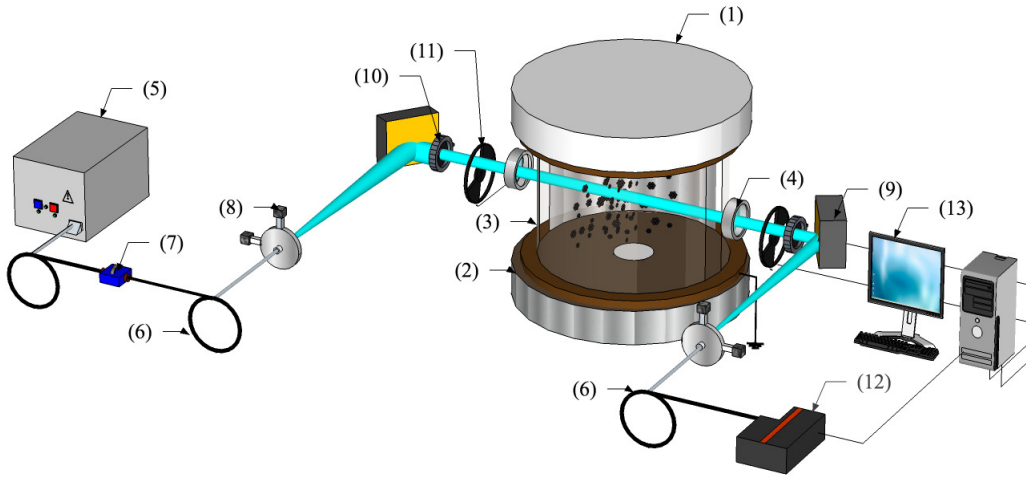

FIGURE 9. Schematic of a typical LES setup implemented on a plasma facility: (1) cathode, (2) grounded anode, (3) glass half cylinders, (4) UV fused silica windows, (5) highly-stabilized Halogen-Deuterium lamp, (6) optical fibers, (7) on-line intensity attenuator, (8) achromatic coupling and collimating optics, (9) parabolic mirrors, (10) diaphragm, (11) optical choppers, (12) UV-NIR spectrometer, (13) computer.

It was developed to study the growth of tungsten and silicon nanoparticles produced in low pressure discharges (Onofri *et al.* 2011; Barbosa *et al.* 2016). This setup has also been used to characterize aerosols of buckyball shaped SiO_2 nanoagregates (Onofri *et al.* 2013) and aerosols of compact tungsten aggregates in the perspective to develop combined laser induced breakdown spectroscopy (LIBS) and LES measurements in fusion devices (Onofri *et al.* 2012).

This set-up is composed of a highly-stabilized Halogen-Deuterium lamp (a DH-2000-DUV from Ocean Optics), solarisation resistant optical fibers with a 200 μm core, an on-line intensity attenuator, achromatic coupling and collimating optics (50 mm focal

length parabolic mirrors), a diaphragm to control the diameter of the probed zone (and thus refine the spatial resolution of the system), a low noise and high dynamic CCD spectrometer (a Maya Pro from Oceans Optics). This spectrometer has an enhanced response in the UV range and a global half-height resolution of 25 nm. Depending of the optical windows installed on the plasma chamber, the effective spectral range of the full system is about $\lambda = 200 - 1000$ nm. The aperture angle of the detection system is smaller than 0.1^o, allowing to neglect the scattering of particles with diameter smaller than $\sim 2\,\mu$m. In all situations, and as a prerequisite to calculate the transmittance defined in equation 2.1, the background noise and the reference signal are measured before the plasma ignition. In some situations (long-term experiments, huge plasma light emission, ect.), two optical choppers are used to chop periodically and alternatively the probing beam and the collection optics field of view. This procedure allows measuring successively: the optical and electronic signal, the plasma light emissions and the measurement signal. Classically, to further improve the SNR, the final LES spectra is obtained by averaging ~ 20 to ~ 200 instantaneous spectra (the minimum exposure time: 6 ms is selected to further improve the SNR). This procedure decreases the nominal spectrometer acquisition rate from ~ 160 spectra per second down to ~ 2 and even ~ 0.5 spectra per second if the choppers are used. All the control of the system and the computations (i.e. spectrometer, choppers, inversion) are performed with a laptop computer.

3. Parameter range and limitations of the technique

It is extremely difficult to define precisely the parameter range and accuracy of LES in terms of particle size and particle concentration ranges. In fact, they depend on many factors: the optical properties of the particle material (and the knowledge we have of them), the probing length, the SNR of the experiment (light source, CCD, plasma emission,...), the stability of the regularization and inversion algorithm, the appropriateness of the electromagnetic light scattering models and particle shape models, etc. Thus, in the following, we restrict ourselves to some general remarks on the expected size range and particle concentration range for a typical LES set-up like the one described in §2.5. The maximum particle size range of LES is between $\sim \lambda_{min}/20$ to $\sim 5\lambda_{max}$, i.e. ~ 10 nm and $\sim 5\,\mu$m for a spectral range of $\sim 200 - 1000$ nm. However, from our experience, the dynamic of a single measurement can hardly exceed $D_{max}/D_{min} \sim 20 - 30$. The lower particle size bound comes from the increasing sensitivity of LES to the particle refractive index (specially the imaginary part) at the expense of the particle size while, correlatively, the useful part of the spectrum is becoming narrower (see Figure 13(a)). This makes the inversion procedure very unstable. For the upper bound, the main limiting factor is the evolution of the extinction coefficients itself. This coefficient tends toward 2 for large size parameters (Bohren & Huffman 1998), making LES spectra lesser sensitive to the particle size. One additional limitation for the upper bound is in the intensity of the forward diffraction peak, which rapidly increases with the particle size, polluting increasingly the extinction signal. Although, there exist some correction methods to account for the particle scattering (Deepak & Box 1978*a*,*b*; Hirleman 1988), the problem becomes rapidly insoluble if LES is not coupled with another technique.

The particle concentration range is limited towards the smaller values by the SNR of the system. Optically, the SNR of LES spectra can only be improved by increasing the probing length L. Generally speaking, L can be increased using a multipass optical cell (e.g (Widmann *et al.* 2005))or a resonant optical cavity (e.g. CRDS (Butler *et al.* 2007)). However, these two classical solutions are difficult to implement on plasma facilities and/or when in-situ measurements are required. In addition, losses in the multipass op-

tical cells tend to rapidly decrease the probing beam intensity, when resonant optical cavities operate on a spectral bandwidth (e.g. a few nanometers or tens nanometers) too narrow to perform LES inversions. Therefore, a better approach for characterizing particles in low concentration is to improve LES signal detection and processing schemes (e.g. cross-correlation with a multichannel spectrometer), reduce the spectrometer noise (e.g. cooled CCD), increase LES probing beam energy (e.g. supercontinum light source), etc. The maximum particle concentration is limited by the particle cloud scattering (single or multiple) (Hirleman 1988). This limit can be extended by decreasing the probing length L (e.g. analysis of the plasma edge), reducing the detection system collection angle in order to performe LES analysis only on ballistic photons (Calba *et al.* 2008). As orders of magnitude, based on the experimental conditions reported in §4., the measurement range of LES in term of particle concentrations in volume is found to be in the range of few parts-per-billion to few parts-per-million.

4. Examples of in-situ measurements and comparisons with other techniques

4.1. *Characterisation of tungsten nanoparticle growth in a low pressure discharge*

In this experiment (Barbosa *et al.* 2016), Tungsten nanoparticles were grown in a DC argon glow discharge initiated between a circular tungsten cathode with a diameter of 10 cm and a stainless-steel grounded anode. A detailed description of the set-up and conditions can be found in (Couëdel *et al.* 2014); here only a short summary is proposed. The inter-electrode distance is 10 cm. Two glasses half-cylinders are used to confine the plasma. A 1 cm gap is kept between them to allow the implementation of optical diagnostics. A static argon pressure of 0.6 mbar (no gas flow) is set during the experiments. The electrode assembly is contained in a cylindrical vacuum chamber of 30 cm diameter and 40 cm length. An oil diffusion pump achieves a base pressure of $< 10^{-6}$ mbar. A manually operated gate valve is used to isolate the chamber from the oil diffusion pump during experiments. A regulated power supply is used to bias the cathode. The discharge current density is kept at a constant value (0.53 mAcm^2 corresponding to a current of 40 mA). The current variations are less than 0.05%. The discharge parameters are such that the plasma mainly consisted of a negative glow. With the aforementioned operating conditions, the cathode is sputtered and tungsten NPs are grown (Kishor *et al.* 2013).

As complementary measurements, electron microscopy and Raman spectroscopy analyses were performed (off-line) on particles collected on a movable substrate holder. It turns out that the nanoparticles are roughly spherical, and look mainly like compact aggregates of tungsten crystallites (see Figure 1(a-b)). These observations as well as numerical simulations with rigorous electromagnetic models, justify the choice for LES inversions of the sphere as the particle shape model and the selection of the Lorenz-Mie theory to calculate the extinction matrix. Since the measured transmissions are quite noisy, due to a relatively low particle concentration, only selected values are used for the inversion procedure (see Figure 10(b)). For the same reason, a dependant model is used to help in the regularization problem. Finally, due to the dynamics of the particle cloud, the PSDs in number and in volume is assumed to be of mono-modal or bi-modal log-normal types (Barbosa *et al.* 2016).

Figure 11 shows, typical time series measured with LES at a height of $h = 2.8$ cm for (a) the mean diameters and the associated standard-deviations of each PSD mode and (b) the particle concentrations in number. Note that LES spectra were too noisy before $t \sim 80$ s to allow any reliable inversion. The sudden change of the PSD from mono-modal

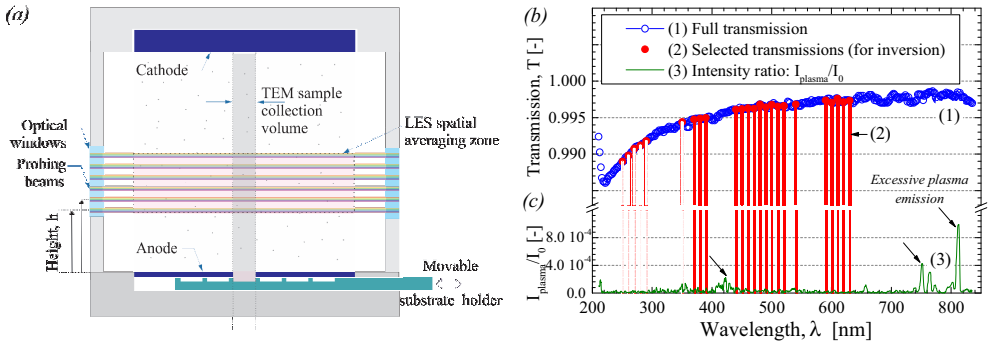

FIGURE 10. Tungsten particle growth. (a) Schematic of the plasma chamber with the probing zones of LES and the particle collection system. (b) Typical raw spectrum and values selected for the inversion at $h = 5.3$ cm and $t = 100$ s. (c) Intensity ratio of the plasma emission collected by LES system with respect to the probing beam intensity.

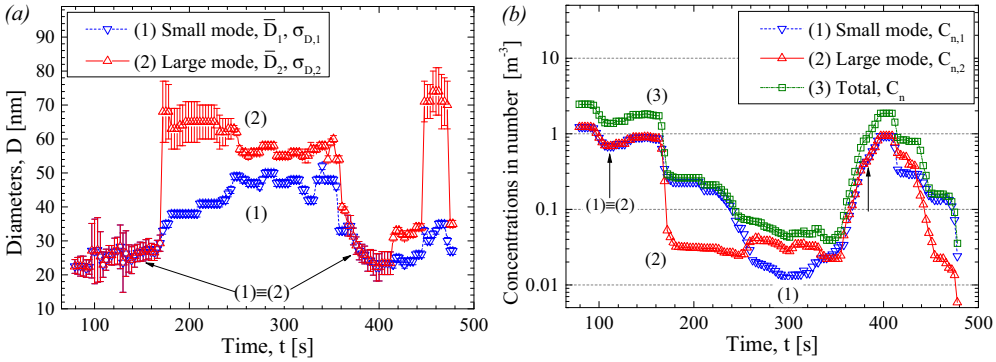

FIGURE 11. Tungsten particle growth - LES measurements. (a) Temporal evolution of the mean diameter and associated standard-deviation (represented by bars) of each PSD mode for $h = 2.8$ cm from the anode. (b) Corresponding evolution for the particle cloud concentration in number (small and large modes, total) (Barbosa *et al.* 2016).

to bi-modal observed in Figure 11 a) is attri to an agglomeration process. The large mode corresponds to the agglomeration of ~ 35 nm particles at constant volume (Barbosa *et al.* 2016), when the small mode is constituted by particles of a first generation that are not totally consummated by the agglomeration process and remain in the LES probing zone. Figure 12(a) shows the evolution of the statistical moments of the PSD in number for different heights above the anode and when the minimum of transmittance is reached (i.e. corresponding to the opening of a "dust free" region in the LES beam, for example at 230 s for $h = 2.8$ cm and at 170 s for $h = 5.3$ cm) (Barbosa *et al.* 2016). It can be clearly seen that the agglomeration process and cloud properties are not homogeneous in the discharge (this was confirmed qualitatively by laser tomography images). The mean size of the nanoparticles belonging to the large mode increases when getting closer to the anode, while on the contrary, the mean size associated to the small mode shows no clear trend. These result suggest that the agglomeration process is triggered when the biggest nanoparticles fall through a cloud of smaller nanoparticles and grow until they reach the anode side.

Figure 12(b) illustrates the difficulty when comparing in-situ and ex-situ analyses. On one hand, TEM analyses are performed on a sample that is expected to be represen-

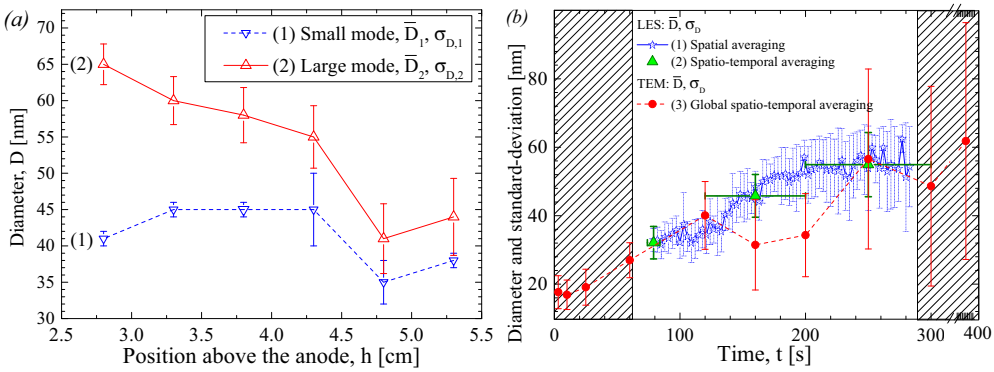

FIGURE 12. Tungsten particle growth. (a) Evolution with the height above the anode of the mean diameter and the associated standard-deviation (represented by bars) of each PSD mode, measured with LES at the minima in transmittance. (b) Comparison of TEM statistics with LES statistics (spatially averaged over $h = 2.8$ to $h = 5.3$ cm, plus time averaged over the time required to collect the samples).

tative of particle populations within, more or less, a cylindrical volume defined by the particle sample collection system area and the full electrodes inter-distance (as sketched in Figure 10(a)). The sample collection procedure takes time and several discharges are necessary to collect enough particles. Thus, TEM results must be considered as spatio-temporal averaged quantities. On the other hand, LES provides time-resolved statistics representative of the particle cloud properties at a given height. For a better comparison, LES analyses should be performed (and spatially averaged) over the whole electrode gap. Unfortunately, this was not possible on the current plasma test chamber and indeed, only one third of this distance was accessible for the experiments reported here. Figure 12(b) shows LES global results obtained with these spatial-averaging (for $h = 2.8$ to 5.3 cm) and time-averaging (over the time required to collect TEM samples, "spatio-temporal averaging" case) procedures. The results are in a qualitative agreement, despite significant fluctuations of the TEM analyses on collected samples. Note that for these mean calculations LES maximum acquisition time was limited by the shortest time series recorded (i.e. 300 s).

4.2. *Silicium nanoparticle formation in an argon-silane low pressure radio-frequency plasma*

In this experiment (Onofri *et al.* 2011), silicon nanoparticles were grown in a transient low-pressure argon-silane radio-frequency (RF) discharge where the total pressure ~ 13 mBar, the RF electrode power ~ 10 W and the mass fraction $Y_{SIH4/Ar} = 4\%$ were maintained constant during all the experiment duration. The LES system was installed on both sides of the chamber (Onofri *et al.* 2011) with a probing beam positioned halfway between the electrodes. A detailed description of the setup and conditions can be found. We summarize here the basic parameters of the plasma test chamber. The discharge is confined in a grounded cylindrical (13 cm diameter) stainless steel box. The shower type upper electrode (driven electrode) is connected to a standard matching box, supplied with Argon and Silane (SiH_4, in order to ensure a good homogeneity of the gas mixture at the entrance of the discharge gap. The inter-electrode distance is about 3.3 cm. A grid (50% of transparency) is placed at the bottom of the grounded box in order to obtain a laminar vertical gas flow. The discharge structure is enclosed in a vacuum chamber

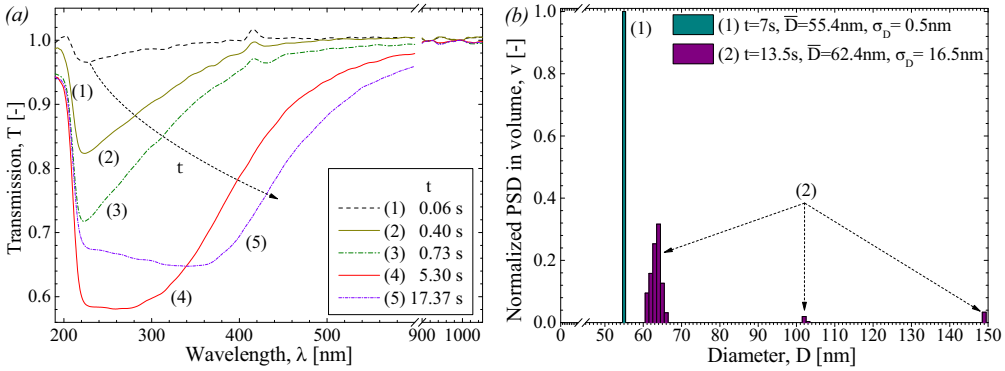

FIGURE 13. Silicon particle growth. (a) LES transmissions measured at different times t after the plasma ignition; (b) two characteristic PSDs in volume extracted from the time series (see Figure 14).

(30 cm height, 30 cm diameter) containing two UV fused silica windows for optical diagnostics. The particle sample collection system for ex-situ TEM/SEM analyses is set at the center of the bottom electrode.

Complementary analyses show that the nanoparticles formed in the discharge take the form of dense aggregates (see Figure 1(c-d)) composed of monomers with apparently nanocristallites inclusions embedded in an amorphous matrix. They are essentially composed of silicon (Si), with a small fraction in mass of hydrogen. These observations justify the selection of a high compactness fractal-like aggregate model for the particle shape model (with $D_f = 2.85$, $r_p = 3.5$ nm and $n_p = 1, 2, ...813$). To account for their composition, the refractive index of several forms of silicon is to be tested: amorphous, crystalline, polysilicon,... (SOPRA 2008) as well as their different mixtures. When compared to TEM analyses, the best agreement is obtained when using the refractive index spectra of amorphous silicon. Thus, in the following, to solve the direct and the inverse problems, the T-Matrix and Twomey-Philips methods are used with the cross-section diameter (i.e. $D \equiv D_A$) and the refractive index of amorphous silicon.

Typical evolutions for LES spectra are shown in Figure 13(a), for different time t after the plasma ignition ($t = 0$ s). In Figure 13(a) and for $t < 1$ s, the transmission is always above ~ 0.7 for 220 nm $< \lambda <$ 500 nm, indicating that small particles are already produced. For increasing time, the minimum of the transmission decreases and is shifted towards higher wavelengths. Generally speaking, these two trends are the signature of an increase of the particle size. Figure 13(b) shows two PSD obtained for $t \sim 6.5$ s and 13 s. Figure 14 shows the temporal evolution of (a) the two first statistical moment of the PSD in volume and (b) the corresponding concentrations in number and volume. For $t < 8 - 9$ s, the mean diameter increases rapidly, while the standard-deviation remains extremely small ($\sigma_D < 1$). While LES predicts narrower size distributions, a good agreement is found for the mean diameter when compared to TEM analyses performed for the same conditions: a decade before (case noted 2 in Figure 14(a) (Boufendi & Bouchoule 1994) and a few months after (case noted 3) experiments carried with LES. The latter observation on the PSD width is explained, as for the tungsten particles, by the fact that LES measurements are representative of the particle cloud properties at a given height in the discharge, whereas TEM measurements are integrated over a larger volume and a longer time. The statistics are thus not directly comparable except when the particle cloud properties are spatially homogeneous in all the discharge. For $t > 8 - 9$ s, the mean diameter tends to be nearly constant while the standard-deviation increases significantly

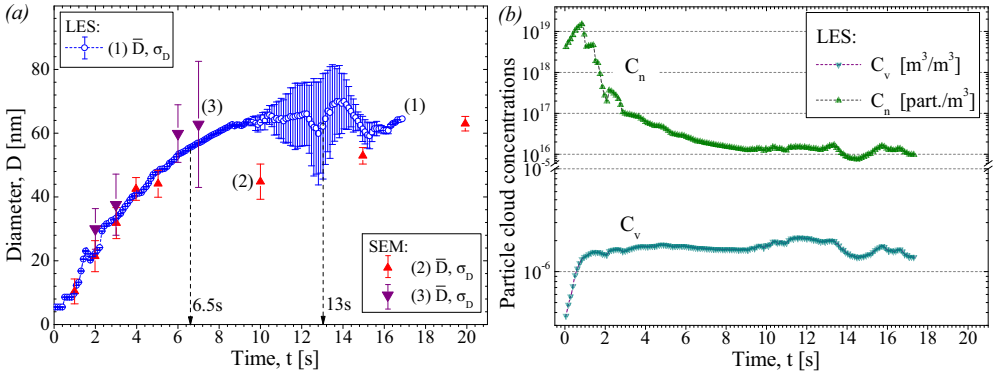

FIGURE 14. Silicon particle growth. (a) Comparison of the time evolution of the mean diameter and the associated standard-deviation (represented as bars) measured with (1) LES and (2-3) TEM analyses. (b) Corresponding evolution for the particle cloud concentrations in number and in volume measured with LES.

prior to diminish above $t \sim 15 - 16$ s. For $t \sim 10 - 12$ s, LES and TEM analyses do not match as well as before. The standard-deviation estimated by LES is for instance significantly higher. This discrepancy may be explained by a vertical stratification of the particle cloud properties, but also by the fact that LES has detected two other populations of particles, like shown by Figure 13(b). Their statistical weights are probably too weak to be observed with electron microcopy analyses based on a hundred particles. The discrepancy on the mean diameter is harder to explain, and espacially because a better agreement is found later on. Slight variations in the control of the discharge, from one experiment to another one, some arc discharges introducing some instabilities in the process, are two plausible explanations for this punctual deviation.

5. Conclusion

In this article, the physical basis and basic equations of the LES technique are reviewed including all the modeling aspects connected to the inversion problem (regularization methods, particle shape, refractive index and electromagnetic models). Then, the parameter range and limitations of the technique are discussed although it is stressed that they highly depend on the particle system studied. A basic experimental set-up is described, including hardware and software requirements, with some perspectives regarding future developments and refinements. Finally, examples of measurements in two types of low-pressure gas discharges are presented. A special emphasis is given on the reasons that have guided the selection of the most appropriate models for data inversion, together with warnings on interpretation of the results obtained.

To conclude, it is thought that LES is a powerful technique for in-situ and real time characterization of complex shaped and polydisperse nano- to micro-sized particle in reactive plasmas. It provides particle size distributions and concentrations (absolute). It requires only two optical access, facing each other and which size depend mostly of the discharge region to be probed). It is also relatively simple to implement as well as rather inexpensive. These features make this technique very appealing and unique. The necessity to have a certain prior knowledge on the particle composition and shape is a difficult issue. However, this is a common limitation of all inverse techniques.

Acknowledgements - This work was partially supported by the INSIS of CNRS (grant PEPS, Projets Exploratoires Premier Soutien), the French National Research (grant ANR-09-BLAN-023-01), the Federation for Magnetic Confinement Fusion (FR-FCM) in collaboration with the Association Euratom- CEA (grant V3485.001).

REFERENCES

Asano, S. & Yamamoto, G. 1975 Light scattering by a spheroidal particle. *Applied optics* **14** (1), 29–49.

Aster, R. C., Borchers, B. & Thurber, C. H. 2012 *Parameter Estimation and Inverse Problems*, *International Geophysics*, vol. 90. Cambridge, MA: Academic Press.

Barbosa, S., Couëdel, L., Arnas, C., Kumar, K. Kishor, Pardanaud, C. & Onofri, F. R. A. 2016 In-situ characterisation of the dynamics of a growing dust particle cloud in a direct-current argon glow discharge. *Journal of Physics D: Applied Physics* **49** (4), 045203.

Berndt, J., Kovačević, E., Stefanović, I., Stepanović, O., Hong, S. H., Boufendi, L. & Winter, J. 2009 Some aspects of reactive complex plasmas. *Contributions to Plasma Physics* **49** (3), 107–133.

Bohren, C. F. 1986 Applicability of effective-medium theories to problems of scattering and absorption by nonhomogeneous atmospheric particles. *Journal of the Atmospheric Sciences* **43** (5), 468–475.

Bohren, C. F. & Huffman, D. R. 1998 *Absorption and scattering of light by small particles*. New york: Wiley & Sons.

Borghese, F., Denti, P. & Saija, R. 1994 Optical properties of spheres containing several spherical inclusions. *Applied optics* **33** (3), 484–493.

Boufendi, L. & Bouchoule, A. 1994 Particle nucleation and growth in a low-pressure argon-silane discharge. *Plasma Sources Science and Technology* **3** (3), 262.

Butler, T. J. A., Miller, J. L. & Orr-Ewing, A. J. 2007 Cavity ring-down spectroscopy measurements of single aerosol particle extinction. i. the effect of position of a particle within the laser beam on extinction. *The Journal of Chemical Physics* **126** (17), 174302.

Calba, C., Méès, L., Rozé, C. & Girasole, T. 2008 Ultrashort pulse propagation through a strongly scattering medium: simulation and experiments. *Journal of the Optical Society of America A* **25** (7), 1541–1550.

Chakrabarty, R.K. et al. 2009 Low fractal dimension cluster-dilute soot aggregates from a premixed flame. *Phys. Rev. Lett.* **102**, 235504.

Couëdel, L., Kumar K., Kishor & Arnas, C. 2014 Detrapping of tungsten nanoparticles in a direct-current argon glow discharge. *Physics of Plasmas* **21** (12), 123703.

Crawley, G., Cournil, M. & Di Benedetto, D. 1997 Size analysis of fine particle suspensions by spectral turbidimetry : Potential and limits. *Powder Technol.* **91**, 197–208.

Deepak, A. & Box, M. A. 1978*a* Forwardscattering corrections for optical extinction measurements in aerosol media. 1: Monodispersions. *Applied optics* **17** (18), 2900–2908.

Deepak, A. & Box, M. A. 1978*b* Forwardscattering corrections for optical extinction measurements in aerosol media. 2: Polydispersions. *Applied optics* **17** (18), 3169–3176.

Dobbins, R. A. & Megaridis, C. M. 1991 Absorption and scattering of light by polydisperse aggregates. *Applied optics* **30** (33), 4747–4754.

Dominique, C. & Arnas, C. 2007 Cathode sputtering and the resulting formation of carbon nanometer-size dust. *Journal of Applied Physics* **101** (12), 123304.

Draine, B. T. & Flatau, P. J. 1994 Discrete-dipole approximation for scattering calculations. *Journal of the Optical Society of America A* **11** (4), 1491–1499.

Farias, T. L., Köylü, Ü Ö & Carvalho, M. G. 1996 Range of validity of the rayleigh–debye–gans theory for optics of fractal aggregates. *Applied optics* **35** (33), 6560–6567.

Gebauer, G & Winter, J 2003 In situ nanoparticle diagnostics by multi-wavelength rayleigh-mie scattering ellipsometry. *New Journal of Physics* **5**, 38.

Glasse, B., Riefler, N. & Fritsching, U. 2015 Intercomparison of numerical inversion algorithms for particle size determination of polystyrene suspensions using spectral turbidimetry. *Journal of Spectroscopy* **2015**, 10.

Guinier, A., Fournet, G., Walker, C. B. & Yudowitch, K. L. 1995 *Small Angle Scattering of X-Rays*. New-York: Wiley.

Hansen, P. C. 1994 Regularization tools, a matlab package for analysis and solution and solution of discrete ill-posed problems. *Numerical Algorithms* **6** (1), 1–35.

Hansen, P. C. 1998 *Rank-Deficient and Discrete Ill-Posed Problems: Numerical Aspects of Linear Inversion. Mathematical Modeling and Computation* xx. Philadelphia, PA: SIAM.

Hansen, P. C., Pereyra, V. & Scherer, G. 2012 *Least Squares Data Fitting with Applications*. Baltimore, MA: Johns Hopkins University Press.

Hirleman, D. E. 1988 Modeling of multiple scattering effects in fraunhofer diffraction particle size analysis. *Particle & Particle Systems Characterization* **5** (2), 57–65.

Hong, S., Berndt, J. & Winter, J. 2003 Growth precursors and dynamics of dust particle formation in the Ar/CH4 and Ar/C2H2 plasmas. *Plasma Sources Science and Technology* **12** (1), 46.

Hong, S. H. & Winter, J. 2006 Size dependence of optical properties and internal structure of plasma grown carbonaceous nanoparticles studied by in situ rayleigh-mie scattering ellipsometry. *Journal of Applied Physics* **100** (6), 064303.

Jäger, C., B. Il'in, V., Henning, T., Mutschke, H., Fabian, D., Semenov, A. D. & Voshchinnikov, V. N. 2003 A database of optical constants of cosmic dust analogs. *Journal of Quantitative Spectroscopy and Radiative Transfer* **79-80**, 765–774.

Jullien, R. & Botet, R. 1987 *Aggregation and Fractal Aggregates*. Singapore: World Scientific.

Kaye, B. H. 1994 *A Random Walk Through Fractal Dimensions*. New York: Weinheim.

King, M. D., Byrne, D. M., Herman, B. M. & Reagan, J. A. 1978 Aerosol size distributions obtained by inversions of spectral optical depth measurements. *Journal of the Atmospheric Sciences* **35** (11), 2153–2167.

Kishor, Kumar K., Couëdel, L. & Arnas, C. 2013 Growth of tungsten nanoparticles in direct-current argon glow discharges. *Physics of Plasmas* **20** (4), 043707.

Ku, J. C. & Felske, J. D. 1986 Determination of refractive indices of mie scatterers from kramers–kronig analysis of spectral extinction data. *Journal of the Optical Society of America A* **3** (5), 617–623.

Mackowski, D. W. & Mishchenko, M. I. 1996 Calculation of the t matrix and the scattering matrix for ensembles of spheres. *Journal of the Optical Society of America A* **13** (11), 2266–2278.

Meakin, P. 1983 Formation of fractal clusters and networks by irrevesible diffusion-limited aggregation. *Physical Review Letters* **51** (13), 1119–1122.

Mishchenko, M.I. & Travis, L.D. 2010 Electromagnetic scattering by particles and surfaces (NASA GISS). http://www.giss.nasa.gov/staff/mmishchenko/.

Mishchenko, M. I., Dlugach, Z. M. & Zakharova, N. T. 2014 Direct demonstration of the concept of unrestricted effective-medium approximation. *Optics Letters* **39** (13), 3935–3938.

Mishchenko, M. I., Hovenier, J. W. & Travis, L. D. 2000 *Light Scattering by Non Spherical Particles: Theory, Measurements and Applications*. San Diego, USA: Academic Press.

Mishchenko, M. I. & Martin, P. A. 2013 Peter Waterman and T-Matrix methods. *J. Quant. Spectrosc. Radiat. Transfer* **123**, 2–7.

Mitic, S., Pustylnik, M. Y., Morfill, G. E. & Kovačević, E. 2011 In situ characterization of nanoparticles during growth by means of white light scattering. *Opt. Lett.* **36** (18), 3699–3701.

Mroczka, J., Wozniak, M. & Onofri, F. R. A. 2012 Algorithms and methods for the analysis of the optical structure factor of fractal aggregates. *Metrology and Measurement Systems* **XIX** (3), 459–470.

Muinonen, K., Nousiainen, T., Fast, P., Lumme, K. & Peltoniemi, J. I. 1996 Light scattering by gaussian random particles: Ray optics approximation. *Journal of Quantitative Spectroscopy and Radiative Transfer* **55** (5), 577–601.

Onofri, F. & Barbosa, S. 2012*a* Basics on light scattering properties of small particles. In *Laser Metrology in Fluid Mechanics* (ed. A. Boutier). London: Wiley-ISTE.

Onofri, F. & Barbosa, S. 2012*b* Optical particle characterization. In *Laser Metrology in Fluid Mechanics* (ed. A. Boutier). London: Wiley-ISTE.

Onofri, F., Gréhan, G. & Gouesbet, G. 1995 Electromagnetic scattering from a multilayered sphere located in an arbitrary beam. *Applied optics* **34** (30), 7113–7124.

Onofri, F., Ren, K. F. & Grisolia, C. 2009 Development of an in situ ITER dust diagnostic based on extinction spectrometry: Dedicated light scattering models. *Journal of Nuclear Materials* **390–391**, 1093–1096.

Onofri, F. R. A., Barbosa, S., Touré, O., Woźniak, M. & Grisolia, C. 2013 Sizing highly-ordered buckyball-shaped aggregates of colloidal nanoparticles by light extinction spectroscopy. *Journal of Quantitative Spectroscopy and Radiative Transfer* **126**, 160–168.

Onofri, F. R. A., Barbosa, S., Wozniak, M., Vrel, D. & Grisolia, C. 2012 In-situ characterization of dust mobilized by laser cleaning methods and loss of vacuum accident. *Fusion Science and Technology* **62** (1), 39–45.

Onofri, F. R. A., Wozniak, M. & Barbosa, S. 2011 On the optical characterisation of nanoparticle and their aggregates in plasma systems. *Contributions to Plasma Physics* **51** (2-3), 228–236.

Palik, E. D. 1997 *Handbook of Optical Constants of Solids*. Burlington: Academic Press.

Phillips, D. L. 1962 A technique for the numerical solution of certain integral equations of the first kind. *Journal of the ACM* **9** (1), 84–97.

POV-Ray 2010 The Persistence of Vision Raytracer Pty. Ltd. http://www.povray.org/.

Rosanvallon, S., Grisolia, C., Counsell, G., Hong, S. H., Onofri, F., Worms, J., Winter, J., Annaratone, B. M., Maddaluno, G. & Gasior, P. 2008 Dust control in tokamak environment. *Fusion Engineering and Design* **83**, 1701–1705.

Rosanvallon, S., Grisolia, C., Delaporte, P., Worms, J., Onofri, F., Hong, S. H., Counsell, G. & Winter, J. 2009 Dust in ITER: Diagnostics and removal techniques. *Journal of Nuclear Materials* **386-388**, 882–883.

Samsonov, D. & Goree, J. 1999*a* Instabilities in a dusty plasma with ion drag and ionization. *Phys. Rev. E* **59**, 1047.

Samsonov, D. & Goree, J. 1999*b* Particle growth in a sputerring discharge. *J. Vac. Sci. Technol. A* **17** (5), 2835.

Sebastian, Groth, Franko, Greiner, Benjamin, Tadsen & Alexander, Piel 2015 Kinetic mie ellipsometry to determine the time-resolved particle growth in nanodusty plasmas. *Journal of Physics D: Applied Physics* **48** (46), 465203.

Sentis, M. 2014 Modelling and inversion of particle light scattering diagrams recorded with conformable organic photosensors. PhD thesis, Aix-Marseille University, Marseille.

Sentis, M., Onofri, F. R. A., Chauchard, F., Dhez, O. & Laurent, J.Y. 2014 Organic photo sensors: a revolution for the development of innovative particle sizing methods.

Sharpe, J. P., Petti, D. A. & Bartels, H. W. 2002 A review of dust in fusion devices: Implications for safety and operational performance. *Fusion Engineering and Design* pp. 153–163.

SOPRA 2008 Software Spectra, Optical Database from SOPRA SA. http://www.sspectra.com/sopra.html.

Sorensen, C. M. 2001 Light scattering by fractal aggregates: A review. *Aerosol Science and Technology* **35** (2), 648–687.

Tamanai, A., Mutschke, H., Blum, J. & Neuha, R. 2006 Experimental infrared spectroscopic measurement of light extinction for agglomerate dust grains. *Journal of Quantitative Spectroscopy and Radiative Transfer* **100**, 373–381.

Theiler, J. 1990 Estimating fractal dimension. *Journal of the Optical Society of America A* **7** (6), 1055–1073.

Tikhonov, A. N., Goncharsky, A., Stepanov, V. V. & Yagola, A. G. 1995 *Numerical Methods for the Solution of Ill-Posed Problems. Mathematics and Its Applications* xx. Springer Netherlands.

Twomey, S. 1963 On the numerical solution of fredholm integral equations of the first kind by the inversion of the linear system produced by quadrature. *Journal of the ACM* **10** (1), 97–101.

Twomey, S. 1979 *Introduction to the Mathematics in Remote Sensing and Indirect Measurement*. New York: Elsevier.

Waterman, P.C. 1965 Matrix formulation of electromagnetic scattering. *Proc. IEEE* **53** (8), 805–812.

Wattieaux, G., Mezeghrane, A. & Boufendi, L. 2011 Electrical time resolved metrology of dust particles growing in low pressure cold plasmas. *Physics of Plasmas* **18** (9), 093701.

Widmann, J. F., Duchez, J., Yang, J. C., Conny, J. M. & Mulholland, G. W. 2005 Measurement of the optical extinction coefficient of combustion-generated aerosol. *Journal of Aerosol Science* **36** (2), 283–289.

Witten, T. A. & Sander, L. M. 1981 Diffusion-limited aggregation, a kinetic critical phenomenon. *Physical Review Letters* **47** (19), 1400–1403.

Wozniak, M. 2012 Characterization of nanoparticle aggregates with light scattering techniques. Phd thesis, Aix-Marseille University, Marseille.

Wozniak, M. & Onofri, F. R. A. 2012 Modelling the morphology and tem images of fractal aggregates of spherical particles (dla 1.13).

Wozniak, M., Onofri, F. R. A., Barbosa, S., Yon, J. & Mroczka, J. 2012 Comparison of methods to derive morphological parameters of multi-fractal samples of particle aggregates from tem images. *Journal of Aerosol Science* **47**, 12–26.

Wriedt, T. 1998 A review of elastic light scattering theories. *Particle & Particle Systems Characterization* **15** (2), 67–74.

Wriedt, T. 2007 Review of the null-field method with discrete sources. *J. Quant. Spectrosc. Radiat. Transfer* **106**, 535.

Wriedt, T. 2010 Light Scattering Programs (SCATTPORT). http://www.scattport.org/index.php/light-scattering-software.

Wyatt, P. J., Schehrer, K. L., Phillips, S. D., Jackson, C., Chang, Y.J., Parker, R. G., Phillips, D. T. & Bottiger, J. R. 1988 Aerosol particle analyzer. *Applied optics* **27** (2), 217–221.

Xu, R. 2001 *Particle characterization : Light scattering methods*. Dordrecht: Kluwer Academic Publishers.

Yan, B., Zhang, H. & Liu, C. 2012 Scattering of on-axis gaussian beam by a chiral spheroid. *Journal of the Optical Society of America A* **29** (11), 2381–2385.

Yurkin, M. A. & Kahnert, M. 2013 Light scattering by a cube: Accuracy limits of the discrete dipole approximation and the t-matrix method. *Journal of Quantitative Spectroscopy and Radiative Transfer* **123**, 176–183.